JOURNAL OF THEORETICAL
AND APPLIED MECHANICS

ONLINE FIRST

DIFFRACTION OF PLANE *P*-WAVE BY AN UNDERWATER TUNNEL

Jia HA, Guochao LI*, Mingjian YU, Chong NIU, Wanwan FU

Yellow River Engineering Consulting Co., Ltd., Zhengzhou 450003, China
*corresponding author, *algcycg@163.com*

In this investigation, the traditional seismic response problem of tunnels in single-phase and saturated soil under the incidence of plane waves is extended to the ground motion problem considering the overlying water. Firstly, the site model of underwater tunnel under plane P-wave incidence is established. Then, the influence of thermal physical parameters such as incident angle, incident frequency and porosity on the ground motion of an underwater tunnel is studied using the Fourier–Bessel series expansion method of the wave function, which provides a reasonable explanation for the ground motion of an underwater site.

Keywords: saturated soil; underwater tunnel; scattering; plane P-wave; wave propagation.

1. Introduction

As a result of the scarcity of land resources, many cities began to focus on constructing underground facilities. With the construction of ocean engineering, an increasing number of scholars have begun to pay attention to the study of the effect of ground motion on underwater sites. The underwater tunnel is a significant transport terminal-junction. If damaged by the earthquake, it would inevitably cause significant property damage. The essence of the research on the impact of the underwater tunnel on ground motion is to examine the diffraction of the elastic wave, which can simulate the influence of seismic waves on various linear structures. Accordingly, it is significant to investigate the diffraction of seismic waves by underwater tunnels and to examine the influence of topographic conditions on ground motion and the ground motion of underground sites considering local geological structures.

Currently, many scholars have conducted the analysis and research on seismic response problems and achieved important scientific research results. Pao and Mow pioneered the use of the wave function expansion method to investigate the DSCF of a hole in the whole space under seismic wave incidence (Achenbach, 1973). Subsequently, Lee and Karl (1992) extended the method to half space and investigated the analytical solution of plane wave diffraction through a cavity. Luco and de Barros (1994) obtained the two-dimensional response of a circular cavity in a viscoelastic half-space under the action of plane P-wave, SH-wave, SV-wave, and the Rayleigh wave based on the two-dimensional Green's function and the indirect boundary integral method. Gomes *et al.* (2015) investigated the scattering of seismic waves by a circular tunnel in two layers of linear elastic soil using the finite element method. Liang *et al.* (2023) investigated the scattering of plane SH-waves by a circular tunnel in a nonlocal fractional-order viscoelastic half-space by using the complex variable function method.

However, the contents of the above research are the scattering law in the single-phase foundation, without considering the influence of other factors in soil. In fact, owing to the presence of groundwater and air, the state of soil is closer to saturated or unsaturated soil. Subsequently, on the basis of the Biot theory of porous media (Biot *et al.*, 1956a; 1956b), the diffraction of

elastic waves in saturated soil sites has been extensively investigated. Kattis *et al.* (2003) used the boundary integral method to solve the scattering problem of elastic waves by lining and unlined caverns in a saturated full space. Xu *et al.* (2019) investigated the diffraction of a plane wave by a lining tunnel on the basis of the nonlocal Biot theory. Liu *et al.* (2017) made use of the indirect boundary element method (IBEM) to investigate the diffraction for the plane P-wave by a tunnel. Ding *et al.* (2020) gave the analytical solution of the seismic response of lining tunnels under P-wave incidence. Ba *et al.* (2022) used IBEM to investigate the diffraction of a tunnel in a layered site. Xiang *et al.* (2024) investigated the seismic response of the water-rich tunnel under P-wave incidence. Tan *et al.* (2020) used the wave function expansion method to investigate the scattering problem of a plane dilatational wave disturbed by a lined tunnel with an imperfect interface embedded in an infinite unsaturated poro-elastic solid. Yue and Liu (2023) solved the scattering problem of P- and SV-waves by lining tunnels in unsaturated soil using the method of complex variable function. Zhao *et al.* (2024) investigated the scattering of plane P-waves by unlined and single-layer lined tunnels in unsaturated soils using the Fourier–Bessel expansion method of wave functions. The diffraction of local topography under plane wave incidence has been widely investigated (Ma *et al.*, 2023). The above research shows that the diffraction of local topography in porous elastic media is quite different in single-phase media. Therefore, the multiphase effect of soil cannot be ignored in the investigation of seismic response.

It can be seen that the diffraction of plane waves by a single-layer soil foundation has been widely investigated, but there are few investigations on underwater sites. Therefore, it is of engineering significance to research the diffraction of elastic waves by tunnels in underwater saturated soil sites. On the basis of the Biot theory of saturated porous elastic medium, the diffraction law for the P-wave around the underwater tunnel is investigated using the Fourier–Bessel series expansion method of the wave function. Through numerical examples, the effect of incident wave frequency, angle, porosity and buried depth on the displacement amplitude of dynamic stress concentration factor at the water-soil interface and tunnel surface in the underwater tunnel is analyzed.

2. Materials and methods

The underwater tunnel site model is shown in Fig. 1, using the rectangular coordinate system and cylindrical coordinate. The radius and buried depth for the tunnel are a and d, respectively, and the thickness of the water layer is h. The soil medium is saturated porous medium.

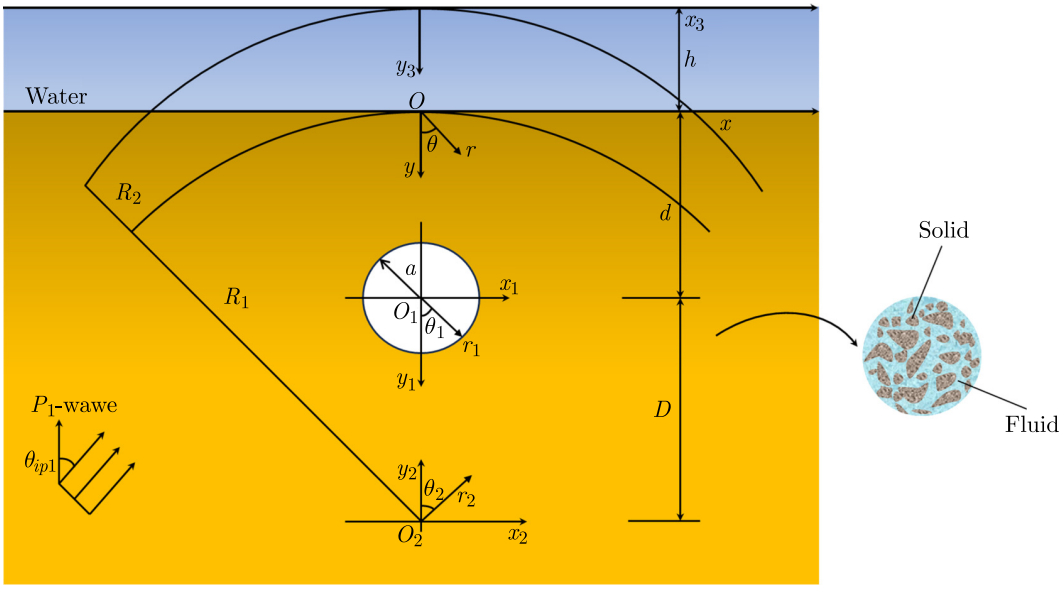

Fig. 1. Model of circular underwater tunnel site.

The constitutive equation and motion equation for the fluid are as follows:

– the constitutive equation:

$$-P_W = K_W \nabla \cdot \mathbf{U}_W, \tag{2.1}$$

– motion equation:

$$K_W \nabla\nabla \cdot \mathbf{U}_W = \rho_W \ddot{\mathbf{U}}_W, \tag{2.2}$$

where P_W is the hydrodynamic pressure of water; K_W denotes the bulk modulus of water; ρ_W denotes the density of water; $\mathbf{U}_W$ denotes the displacement vector of water.

The displacement vector $\mathbf{U}_W$ of the water layer can be written as

$$\mathbf{U}_W = \nabla \varphi_W. \tag{2.3}$$

Equations (2.1) and (2.2) could be expressed by potential functions:

$$-P_W = K_W \nabla^2 \varphi_W, \tag{2.4}$$

$$K_W \nabla^2 \varphi_W = \rho_W \ddot{\varphi}_W^2. \tag{2.5}$$

The wave velocity and wave number of a compression wave in the water layer could be written as

$$c_W = \sqrt{K_W/\rho_W}, \tag{2.6}$$

$$k_W = 2\pi f \sqrt{\rho_W/K_W}. \tag{2.7}$$

For the establishment of the wave equation of saturated soil, referring to the modified Biot model proposed by Zhou *et al.* (2013), which ignores the mass coupling coefficient and considers the compressibility of soil particles and pore fluid, the wave equation of saturated soil is derived from the basic equation of homogeneous saturated porous media.

The wave equation of saturated soil is

$$\mu \nabla^2 u^s + \operatorname{grad}\left[(\mu + \lambda + \alpha^2 M)\theta\right] - \operatorname{grad}(\alpha M \zeta) = \rho \ddot{u}^s + \rho^f \ddot{u}^f, \tag{2.8}$$

$$\operatorname{grad}(\alpha M \theta - M\zeta) = \rho^f \ddot{u}^s + m\ddot{u}^f + b\dot{u}^f. \tag{2.9}$$

According to the Helmholtz vector decomposition theorem, the displacement vector in saturated soil could be expressed as

$$u^s = \nabla \varphi_s + \nabla \times \psi_s, \qquad u^f = \nabla \varphi_f + \nabla \times \psi_f. \tag{2.10}$$

In saturated soil, there are two kinds of compression wave P-waves and one kind of shear wave SV-wave. When P-wave is incident, the circular frequency is ω and the incident angle is θ_{ip1}. The incident wave could be indicated as

$$\varphi_i^\iota(x, y) = A_{ip1}^\iota \exp\left[\mathrm{i}k_{ip1}(x \sin\theta_{ip1} - y\cos\theta_{ip1}) - \mathrm{i}\omega t\right], \tag{2.11}$$

where k_{ip1} is the wave number of P_1-wave, $i = \sqrt{-1}$. $\exp(\mathrm{i}\omega t)$ is left out for simplicity, the aforementioned equations could be expressed as

$$\varphi_i^\iota(x, y) = A_{ip1}^\iota \exp\left[\mathrm{i}k_{ip1}(x \sin\theta_{ip1} - y\cos\theta_{ip1})\right]. \tag{2.12}$$

P-wave will produce reflected P_1-, P_2-, and SV-waves at the water-soil interface, and produce the transmitted P-wave and reflected P-wave in the water. The wave potential functions could be written as:

– in saturated soil:

$$\varphi^{\iota}_{rp1}(x,y) = A^{\iota}_{rp1} \exp\left[\mathrm{i}k_{rp1}(x\sin\theta_{rp1} + y\cos\theta_{rp1})\right], \tag{2.13}$$

$$\varphi^{\iota}_{rp2}(x,y) = A^{\iota}_{rp2} \exp\left[\mathrm{i}k_{rp2}(x\sin\theta_{rp2} + y\cos\theta_{rp2})\right], \tag{2.14}$$

$$\psi^{\iota}_{rs}(x,y) = B^{\iota}_{rs} \exp\left[\mathrm{i}k_{rs}(x\sin\theta_{rs} + y\cos\theta_{rs})\right], \tag{2.15}$$

where k_{rp1}, k_{rp2}, and k_{rs} represent the wavenumbers of reflected P_1-, P_2-, and S-wave, respectively; θ_{rp1}, θ_{rp2}, and θ_{rs} represent the reflection angles. A^{ι}_{rp1}, A^{ι}_{rp2}, and B^{ι}_{rs} represent the amplitude for the reflected waves in ι phase media and $\delta_{L1} = A^{f}_{rp1}/A^{s}_{rp1}$, $\delta_{L2} = A^{f}_{rp2}/A^{s}_{rp2}$.

– in the water layer:

a) transmission P-wave:

$$\varphi^{w}_{i}(x,y) = A^{w}_{tp} \exp\left[\mathrm{i}k_{w}(x_3\sin\theta_{w} - y_3\cos\theta_{w})\right], \tag{2.16}$$

b) reflected P-wave:

$$\varphi^{w}_{rp}(x,y) = A^{w}_{rp} \exp\left[\mathrm{i}k_{rp}(x_3\sin\theta_{w} + y_3\cos\theta_{w})\right], \tag{2.17}$$

where A^{w}_{tp} and A^{w}_{rp} are the amplitude coefficients of the transmitted and the reflected P-waves, respectively, k_w is the wave number of the P-wave in the water, θ_w is the reflection angle of the P-wave in the water layer.

For the convenience of analysis, it can be expressed as follows in cylindrical coordinates:

$$\varphi^{\iota}_{\mathrm{i}}(r_1,\theta_1) = A^{\iota}_{ip1} \exp\left(\mathrm{i}dk_{ip1}\cos\theta_{ip1}\right) \exp\left[-\mathrm{i}k_{ip1}r_1\cos(\theta_1 + \theta_{ip1})\right], \tag{2.18}$$

$$\varphi^{\iota}_{rp1}(r_1,\theta_1) = A^{\iota}_{rp1} \exp\left(-\mathrm{i}dk_{rp1}\cos\theta_{rp1}\right) \exp\left[\mathrm{i}k_{rp1}r_1\cos(\theta_1 - \theta_{rp1})\right], \tag{2.19}$$

$$\varphi^{\iota}_{rp2}(r_1,\theta_1) = A^{\iota}_{rp2} \exp\left(-\mathrm{i}dk_{rp2}\cos\theta_{rp2}\right) \exp\left[\mathrm{i}k_{rp2}r_1\cos(\theta_1 - \theta_{rp2})\right], \tag{2.20}$$

$$\psi^{\iota}_{rs}(r_1,\theta_1) = B^{\iota}_{rs} \exp\left(-\mathrm{i}dk_{rs}\cos\theta_{rs}\right) \exp\left[\mathrm{i}k_{rs}r_1\cos(\theta_1 - \theta_{rs})\right], \tag{2.21}$$

$$\varphi^{w}_{i}(x,y) = A^{w}_{ip} \exp\left[\mathrm{i}k_{w}(d + h\cos\theta_{w}\right] \exp\left[-\mathrm{i}k_{w}\cos(\theta_1 + \theta_{w})\right], \tag{2.22}$$

$$\varphi^{w}_{r}(x,y) = A^{w}_{rp} \exp\left[\text{-}\mathrm{i}k_{w}(d + h\cos\theta_{w}\right] \exp\left[\mathrm{i}k_{w}\cos(\theta_1 - \theta_{w})\right]. \tag{2.23}$$

The aforementioned equation is expanded into the Fourier–Bessel series form:

$$\varphi^{\iota}_{i+rp1}(r_1,\theta_1) = \sum_{n=0}^{\infty} J_n(k_{ip1}r_1)(C_{01,n}\cos n\theta_1 + D_{01,n}\sin n\theta_1), \tag{2.24}$$

$$\varphi^{\iota}_{rp2}(r_1,\theta_1) = \sum_{n=0}^{\infty} J_n(k_{rp2}r_1)(C_{02,n}\cos n\theta_1 + D_{02,n}\sin n\theta_1), \tag{2.25}$$

$$\varphi^{\iota}_{rp3}(r_1,\theta_1) = \sum_{n=0}^{\infty} J_n(k_{rp3}r_1)(C_{03,n}\cos n\theta_1 + D_{03,n}\sin n\theta_1), \tag{2.26}$$

$$\varphi^{w}_{i+r}(r_1,\theta_1) = \sum_{n=0}^{\infty} J_n(k_{w}r_1)(C_{04,n}\cos n\theta_1 + D_{04,n}\cos n\theta_1). \tag{2.27}$$

There are scattered P_1-, P_2-, and SV-waves caused by the tunnel in the saturated soil layer, and scattered P_1-, P_2-, and SV-waves caused by the large arc approximation. The scattered wave

field in a half space could be represented by the Fourier–Bessel series. In the r_1-θ_1 coordinate system, since the scattered wave fields generated by large arcs satisfy the Sommerfeld condition at infinity, their potential functions can be written as the Fourier–Bessel series:

– in saturated soil:

$$\varphi_{dp1}^{\iota}(r_1,\theta_1)=\sum_{n=0}^{\infty}H_n^{(1)}(k_{rp1}r_1)\left(C_{11,n}^{(1)}\cos n\theta_1+D_{11,n}^{(1)}\sin n\theta_1\right), \tag{2.28}$$

$$\varphi_{dp2}^{\iota}(r_1,\theta_1)=\sum_{n=0}^{\infty}H_n^{(1)}(k_{rp2}r_1)\left(C_{12,n}^{(1)}\cos n\theta_1+D_{12,n}^{(1)}\sin n\theta_1\right), \tag{2.29}$$

$$\psi_{ds}^{\iota}(r_1,\theta_1)=\sum_{n=0}^{\infty}H_n^{(1)}(k_{rs}r_1)\left(C_{14,n}^{(1)}\sin n\theta_1+D_{14,n}^{(1)}\cos n\theta_1\right), \tag{2.30}$$

where $J_m(\ )$ and $H_n^{(1)}(\ )$ are the Bessel functions and the Hankel functions, respectively.

The aforementioned equations are established in the (r_1,θ_1) coordinate system, it cannot satisfy the boundary conditions of the water-soil interface and the water layer surface. In this research, the water-soil interface and the free surface of the water layer are simulated by using an arc centred on O_2 (as shown in Fig. 1). Accordingly, the solution in the research is the approximate analytical solution. The research proves that: if the radius of the arc R is sufficiently large ($R>50a$), the error of the calculation result is rather small, and the appropriate result could be obtained.

In the r_2-θ_2 coordinate system, the potential function of the wave generated by the large arc boundary is expressed as follows:

– in saturated soil:

$$\varphi_{ap1}^{\iota}(r_2,\theta_2)=\sum_{m=0}^{\infty}J_m(k_{rp1}r_2)\left(C_{21,n}^{(2)}\cos m\theta_2+D_{21,n}^{(2)}\sin m\theta_2\right), \tag{2.31}$$

$$\varphi_{\mathrm{ap2}}^{\iota}(r_2,\theta_2)=\sum_{m=0}^{\infty}J_m(k_{rp2}r_2)\left(C_{22,n}^{(2)}\cos m\theta_2+D_{22,n}^{(2)}\sin m\theta_2\right), \tag{2.32}$$

$$\psi_{as}^{\iota}(r_2,\theta_2)=\sum_{m=0}^{\infty}J_m(k_{rs}r_2)\left(C_{24,n}^{(2)}\sin m\theta_2+D_{24,n}^{(2)}\cos m\theta_2\right), \tag{2.33}$$

– in the water layer:

$$\varphi_{a1}^{w}(r_2,\theta_2)=\sum_{m=0}^{\infty}J_m(k_wr_2)\left(C_{31,m}^{(2)}\cos m\theta_2+D_{31,m}^{(2)}\sin m\theta_2\right), \tag{2.34}$$

$$\varphi_{a2}^{w}(r_2,\theta_2)=\sum_{m=0}^{\infty}H_m(k_wr_2)\left(C_{32,n}^{(2)}\cos m\theta_2+D_{32,n}^{(2)}\sin m\theta_2\right). \tag{2.35}$$

The total wave potential function can be expressed as follows:

– in saturated soil:

$$\varphi^{\iota}=\varphi_{ip1}^{\iota}+\varphi_{rp1}^{\iota}+\varphi_{rp2}^{\iota}+\varphi_{dp1}^{\iota}+\varphi_{dp2}^{\iota}+\varphi_{ap1}^{\iota}+\varphi_{ap2}^{\iota}, \tag{2.36}$$

$$\psi^{\iota}=\psi_{rs}^{\iota}+\psi_{ds}^{\iota}+\psi_{as}^{\iota}, \tag{2.37}$$

– in the water layer:

$$\varphi^{w}=\varphi_{i}^{w}+\varphi_{r}^{w}+\varphi_{a1}^{w}+\varphi_{a2}^{w}. \tag{2.38}$$

Before introducing the boundary conditions, it is necessary to use the Graf addition formula to unify the coordinates for the wave functions:

$$C_n\left(kr_2\right)\left\{\begin{array}{c}\cos n\theta_2\\ \sin n\theta_2\end{array}\right\}=\sum_{m=-\infty}^{m=+\infty}C_{m+n}\left(kD\right)J_m\left(kr_1\right)\left\{\begin{array}{c}\cos m\theta_1\\ \sin m\theta_1\end{array}\right\}, \tag{2.39}$$

where D is the distance from O_1 point to O_2 point, as shown in Fig. 1, $C_n(\ )$ can be $J_n(\ )$ function or $H_n^{(1)}(\ )$ function.

Therefore, the coordinate transformation of Eqs. (2.28)–(2.43) can be obtained:

$$\varphi_{dp1}^{\iota}(r_2,\theta_2)=\sum_{m=0}^{\infty}J_m(k_{rp1}r_2)\left(C_{11,n}^{(2)}\cos m\theta_2+D_{11,n}^{(2)}\sin m\theta_2\right), \tag{2.40}$$

$$\varphi_{dp2}^{\iota}(r_2,\theta_2)=\sum_{m=0}^{\infty}J_m(k_{rp2}r_2)\left(C_{12,n}^{(2)}\cos m\theta_2+D_{12,n}^{(2)}\sin m\theta_2\right), \tag{2.41}$$

$$\psi_{ds}^{\iota}(r_2,\theta_2)=\sum_{m=0}^{\infty}J_m(k_{rs}r_2)\left(C_{14,n}^{(2)}\sin m\theta_2+D_{14,n}^{(2)}\cos m\theta_2\right), \tag{2.42}$$

$$\varphi_{ap1}^{\iota}(r_1,\theta_1)=\sum_{n=0}^{\infty}J_n(k_{rp1}r_1)\left(C_{21,n}^{(1)}\cos n\theta_1+D_{21,n}^{(1)}\sin n\theta_1\right), \tag{2.43}$$

$$\varphi_{ap2}^{\iota}(r_1,\theta_1)=\sum_{n=0}^{\infty}J_n(k_{rp2}r_1)\left(C_{22,n}^{(1)}\cos n\theta_1+D_{22,n}^{(1)}\sin n\theta_1\right), \tag{2.44}$$

$$\psi_{as}^{\iota}(r_1,\theta_1)=\sum_{n=0}^{\infty}J_n(k_{rs}r_1)\left(C_{24,n}^{(1)}\sin n\theta_1+D_{24,n}^{(1)}\cos n\theta_1\right), \tag{2.45}$$

$$\varphi_{a1}^{w}(r_1,\theta_1)=\sum_{n=0}^{\infty}J_n(k_{w}r_1)\left(C_{31,n}^{(1)}\cos n\theta_1+D_{31,n}^{(1)}\sin n\theta_1\right), \tag{2.46}$$

$$\varphi_{a2}^{w}(r_1,\theta_1)=\sum_{m=0}^{\infty}J_m(k_{w}r_1)\left(C_{32,m}^{(1)}\cos m\theta_1+D_{32,m}^{(1)}\sin m\theta_1\right), \tag{2.47}$$

where

$$\left[\begin{array}{c}C_{11,m}^{(2)}\\ C_{12,m}^{(2)}\\ D_{13,m}^{(2)}\end{array}\right]=\sum_{n=0}^{\infty}\left[\begin{array}{ccc}F2_{nm}^{+}(k_{rp1}D) & & \\ & F2_{nm}^{+}(k_{rp2}D) & \\ & & F2_{nm}^{+}(k_{rs}D)\end{array}\right]\left[\begin{array}{c}C_{11,n}^{(1)}\\ C_{12,n}^{(1)}\\ D_{13,n}^{(1)}\end{array}\right], \tag{2.48}$$

$$\left[\begin{array}{c}D_{11,m}^{(2)}\\ D_{12,m}^{(2)}\\ C_{13,m}^{(2)}\end{array}\right]=\sum_{n=0}^{\infty}\left[\begin{array}{ccc}F2_{nm}^{-}(k_{rp1}D) & & \\ & F2_{nm}^{-}(k_{rp2}D) & \\ & & F2_{nm}^{-}(k_{rs}D)\end{array}\right]\left[\begin{array}{c}D_{11,n}^{(1)}\\ D_{12,n}^{(1)}\\ C_{13,n}^{(1)}\end{array}\right], \tag{2.49}$$

$$\left[\begin{array}{c}C_{21,n}^{(1)}\\ C_{22,n}^{(1)}\\ C_{31,n}^{(1)}\\ C_{32,n}^{(1)}\\ D_{23,n}^{(1)}\end{array}\right]=\sum_{n=0}^{\infty}\left[\begin{array}{ccccc}F1_{nm}^{+}(k_{rp1}D) & & & & \\ & F1_{nm}^{+}(k_{rp2}D) & & & \\ & & F1_{nm}^{+}(k_{w}D) & & \\ & & & F1_{nm}^{+}(k_{w}D) & \\ & & & & F1_{nm}^{+}(k_{rs}D)\end{array}\right]\left[\begin{array}{c}C_{21,m}^{(2)}\\ C_{22,m}^{(2)}\\ C_{31,m}^{(1)}\\ C_{32,m}^{(1)}\\ D_{23,m}^{(2)}\end{array}\right], \tag{2.50}$$

$$\begin{bmatrix} D_{21,n}^{(1)} \\ D_{22,n}^{(1)} \\ D_{31,n}^{(1)} \\ D_{32,n}^{(1)} \\ C_{23,n}^{(1)} \end{bmatrix} = \sum_{n=0}^{\infty} \begin{bmatrix} F1_{nm}^{-}(k_{rp1}D) & & & & \\ & F1_{nm}^{-}(k_{rp2}D) & & & \\ & & F1_{nm}^{-}(k_wD) & & \\ & & & F1_{nm}^{-}(k_wD) & \\ & & & & F1_{nm}^{-}(k_{rs}D) \end{bmatrix} \begin{bmatrix} D_{21,m}^{(2)} \\ D_{22,m}^{(2)} \\ D_{31,m}^{(1)} \\ D_{32,m}^{(1)} \\ C_{23,m}^{(2)} \end{bmatrix}, \tag{2.51}$$

where

$$F1_{nm}^{\pm}(kD) = \frac{1}{2}\varepsilon_n[J_{n+m}(kD) \pm (-1)^m J_{n-m}(kD)],$$

$$F2_{nm}^{\pm}(kD) = \frac{1}{2}\varepsilon_m[H_{m+n}(kD) \pm (-1)^n H_{m-n}(kD)].$$

This research assumes that the surface and the tunnel surface are permeable boundaries, and the boundary conditions are as follows:

– on the surface of the water $y = 0$:

$$\sigma_{rr}^{w} = 0, \tag{2.52}$$

– on the tunnel surface $r_1 = a$:

$$\sigma_{rr}^{S} = 0, \qquad \sigma_{r\theta}^{S} = 0, \qquad \sigma_{rr}^{L} = 0, \tag{2.53}$$

– at the soil-water interface $r_2 = R_1$:

$$(1-n)u_r^S + nu_r^L = u_r^w, \qquad \sigma_{rr}^S + \sigma_{rr}^L = -\sigma_{rr}^w, \qquad \sigma_{rr}^L = -n\sigma_{rr}^w, \quad \sigma_{r\theta}^S = 0. \tag{2.54}$$

Bringing Eq. (2.46) and Eq. (2.47) into the boundary condition (2.52):

$$\sum_{m=0}^{\infty} \begin{bmatrix} E_{11}^{w(1)}(m,R_2) & E_{12}^{w(2)}(m,R_2) \end{bmatrix} \begin{Bmatrix} C_{31,m}^{(2)} \\ C_{32,m}^{(2)} \end{Bmatrix} \{\cos m\theta_2\} + \sum_{m=0}^{\infty} \begin{bmatrix} E_{21}^{w(1)}(m,R_2) & E_{22}^{w(2)}(m,R_2) \end{bmatrix} \begin{Bmatrix} D_{31,m}^{(2)} \\ D_{32,m}^{(2)} \end{Bmatrix} \{\sin m\theta_2\} = \{0\}. \tag{2.55}$$

Bringing Eq. (2.28)–(2.30) and Eq. (2.43)–(2.53) into the boundary condition (2.53):

$$\sum_{m=0}^{\infty} \begin{bmatrix} U_{111}^{s(3)}(n,a) & U_{112}^{s(3)}(n,a) & U_{113}^{s(3)+}(n,a) \\ U_{211}^{s(3)-}(n,a) & U_{212}^{s(3)-}(n,a) & U_{213}^{s(3)}(n,a) \\ U_{311}^{s(3)}(n,a) & U_{312}^{s(3)}(n,a) & 0 \end{bmatrix} \begin{Bmatrix} C_{11,n}^{(1)} \\ C_{12,n}^{(1)} \\ C_{13,n}^{(1)} \end{Bmatrix} \begin{Bmatrix} \cos n\theta_1 \\ \sin n\theta_1 \\ \cos n\theta_1 \end{Bmatrix}$$

$$+ \sum_{m=0}^{\infty} \begin{bmatrix} U_{111}^{s(1)}(n,a) & U_{112}^{s(1)}(n,a) & U_{113}^{s(1)+}(n,a) \\ U_{211}^{s(1)-}(n,a) & U_{212}^{s(1)-}(n,a) & U_{213}^{s(1)}(n,a) \\ U_{311}^{s(1)}(n,a) & U_{312}^{s(1)}(n,a) & 0 \end{bmatrix} \begin{Bmatrix} C_{21,n}^{(1)} + C_{01,n} \\ C_{22,n}^{(1)} + C_{02,n} \\ C_{23,n}^{(1)} + C_{03,n} \end{Bmatrix} \begin{Bmatrix} \cos n\theta_1 \\ \sin n\theta_1 \\ \cos n\theta_1 \end{Bmatrix}$$

$$+ \sum_{m=0}^{\infty} \begin{bmatrix} U_{111}^{s(3)}(n,a) & U_{112}^{s(3)}(n,a) & U_{113}^{s(3)-}(n,a) \\ U_{211}^{s(3)+}(n,a) & U_{212}^{s(3)+}(n,a) & U_{213}^{s(3)}(n,a) \\ U_{311}^{s(3)}(n,a) & U_{312}^{s(3)}(n,a) & 0 \end{bmatrix} \begin{Bmatrix} D_{11,n}^{(1)} \\ D_{12,n}^{(1)} \\ D_{13,n}^{(1)} \end{Bmatrix} \begin{Bmatrix} \sin n\theta_1 \\ \cos n\theta_1 \\ \sin n\theta_1 \end{Bmatrix}$$

$$+ \sum_{m=0}^{\infty} \begin{bmatrix} U_{111}^{s(1)}(n,a) & U_{112}^{s(1)}(n,a) & U_{113}^{s(1)}\text{-}(n,a) \\ U_{211}^{s(1)+}(n,a) & U_{212}^{s(1)+}(n,a) & U_{213}^{s(1)}(n,a) \\ U_{311}^{s(1)}(n,a) & U_{312}^{s(1)}(n,a) & 0 \end{bmatrix} \begin{Bmatrix} D_{21,n}^{(1)} + D_{01,n} \\ D_{22,n}^{(1)} + D_{02,n} \\ D_{23,n}^{(1)} + D_{03,n} \end{Bmatrix} \begin{Bmatrix} \sin n\theta_1 \\ \cos n\theta_1 \\ \sin n\theta_1 \end{Bmatrix} = \begin{Bmatrix} 0 \\ 0 \\ 0 \end{Bmatrix}. \tag{2.56}$$

Bringing Eqs. (2.31)–(2.33) and Eqs. (2.40)–(2.42) into the boundary condition (2.54):

$$\sum_{m=0}^{\infty}\begin{bmatrix} E_{111}^{(s1)} & E_{112}^{(s1)} & E_{113}^{(s1)+} \\ E_{211}^{(s1)} & E_{212}^{(s1)} & E_{213}^{(s1)+} \\ E_{311}^{(s1)} & E_{312}^{(s1)} & 0 \\ E_{411}^{(s1)+} & E_{412}^{(s1)+} & E_{413}^{(s1)} \end{bmatrix}\begin{Bmatrix} C_{11,m}^{(2)}+C_{21,m}^{(2)} \\ C_{12,m}^{(2)}+C_{22,m}^{(2)} \\ C_{13,m}^{(2)}+C_{23,m}^{(2)} \end{Bmatrix}\begin{bmatrix} \cos m\theta_2 \\ \cos m\theta_2 \\ \cos m\theta_2 \\ \sin m\theta_2 \end{bmatrix}$$
$$+\sum_{m=0}^{\infty}\begin{bmatrix} E_{111}^{(s1)} & E_{112}^{(s1)} & E_{113}^{(s1)-} \\ E_{211}^{(s1)} & E_{212}^{(s1)} & E_{213}^{(s1)-} \\ E_{311}^{(s1)} & E_{312}^{(s1)} & 0 \\ E_{411}^{(s1)-} & E_{412}^{(s1)-} & E_{413}^{(s1)} \end{bmatrix}\begin{Bmatrix} D_{11,m}^{(2)}+D_{21,m}^{(2)} \\ D_{12,m}^{(2)}+D_{22,m}^{(2)} \\ D_{13,m}^{(2)}+D_{23,m}^{(2)} \end{Bmatrix}\begin{bmatrix} \sin m\theta_2 \\ \sin m\theta_2 \\ \sin m\theta_2 \\ \cos m\theta_2 \end{bmatrix}$$
$$+\sum_{m=0}^{\infty}\begin{bmatrix} V_{111}^{(s1)} \\ V_{211}^{(s1)} \\ V_{311}^{(s1)} \\ 0 \end{bmatrix}\left\{C_{31,m}^{(2)}\right\}\begin{bmatrix} \cos m\theta_2 \\ \cos m\theta_2 \\ \cos m\theta_2 \\ \sin m\theta_2 \end{bmatrix}+\sum_{m=0}^{\infty}\begin{bmatrix} V_{111}^{(s1)} \\ V_{211}^{(s1)} \\ V_{311}^{(s1)} \\ 0 \end{bmatrix}\left\{D_{31,m}^{(2)}\right\}\begin{bmatrix} \sin m\theta_2 \\ \sin m\theta_2 \\ \sin m\theta_2 \\ \cos m\theta_2 \end{bmatrix}$$
$$+\sum_{m=0}^{\infty}\begin{bmatrix} V_{111}^{(s2)} \\ V_{211}^{(s2)} \\ V_{311}^{(s2)} \\ 0 \end{bmatrix}\left\{C_{32,m}^{(2)}\right\}\begin{bmatrix} \cos m\theta_2 \\ \cos m\theta_2 \\ \cos m\theta_2 \\ \sin m\theta_2 \end{bmatrix}+\sum_{m=0}^{\infty}\begin{bmatrix} V_{111}^{(s2)} \\ V_{211}^{(s2)} \\ V_{311}^{(s2)} \\ 0 \end{bmatrix}\left\{D_{32,m}^{(2)}\right\}\begin{bmatrix} \sin m\theta_2 \\ \sin m\theta_2 \\ \sin m\theta_2 \\ \cos m\theta_2 \end{bmatrix}=\begin{Bmatrix} 0 \\ 0 \\ 0 \\ 0 \end{Bmatrix}, \quad (2.57)$$

where $i = 1$ and 3, $C_n^{(i)}$ is $J_n(x)$ and $H_n^{(1)}(x)$.

The coefficients can be obtained by combining Eqs. (2.55), (2.56), and (2.57).

3. Verification

Converting frequency into dimensionless frequency:

$$\eta = 2a/\lambda_\beta. \quad (3.1)$$

The astringency for the displacement field series could be determined in accordance with the Cauchy criterion:

$$e(n; r_1, \theta_1) = |u(n+1; r_1, \theta_1) - u(n; r_1, \theta_1)|. \quad (3.2)$$

You (2005) investigated the diffraction of P-wave by underground tunnels. For the purpose of validating the result of this research, the underwater tunnel model is degraded to an underground tunnel model in saturated soil. The detailed parameters are shown in (You, 2005), and compared to the displacement derived by You using the IBEM. It could be found out from Fig. 2a that the data is rather consistent, verifying the correctness of the solutions in this research.

In order to further verify the solution of this paper, the underwater tunnel is degraded into a saturated soil depression terrain, and compared with the surface displacement amplitude obtained by Ba (2006) using the large arc assumption. It can be seen from Fig. 2b that the two are in good agreement, which further verifies the correctness of the results in this paper.

If $R = 10^7 a$ it is ample to satisfy the accuracy requirements. The relationship between the error e and the truncation term number n is computed. Figure 3 shows the relationship from the x-, y-direction displacement error e_x, e_y to the n. To satisfy $e_x < 10^{-6}$, in Figs. 3a and 3b, n satisfies $n \geq 14$ and $n \geq 15$, respectively. To sum up, the number of astringency terms of the series is $n_c = 15$.

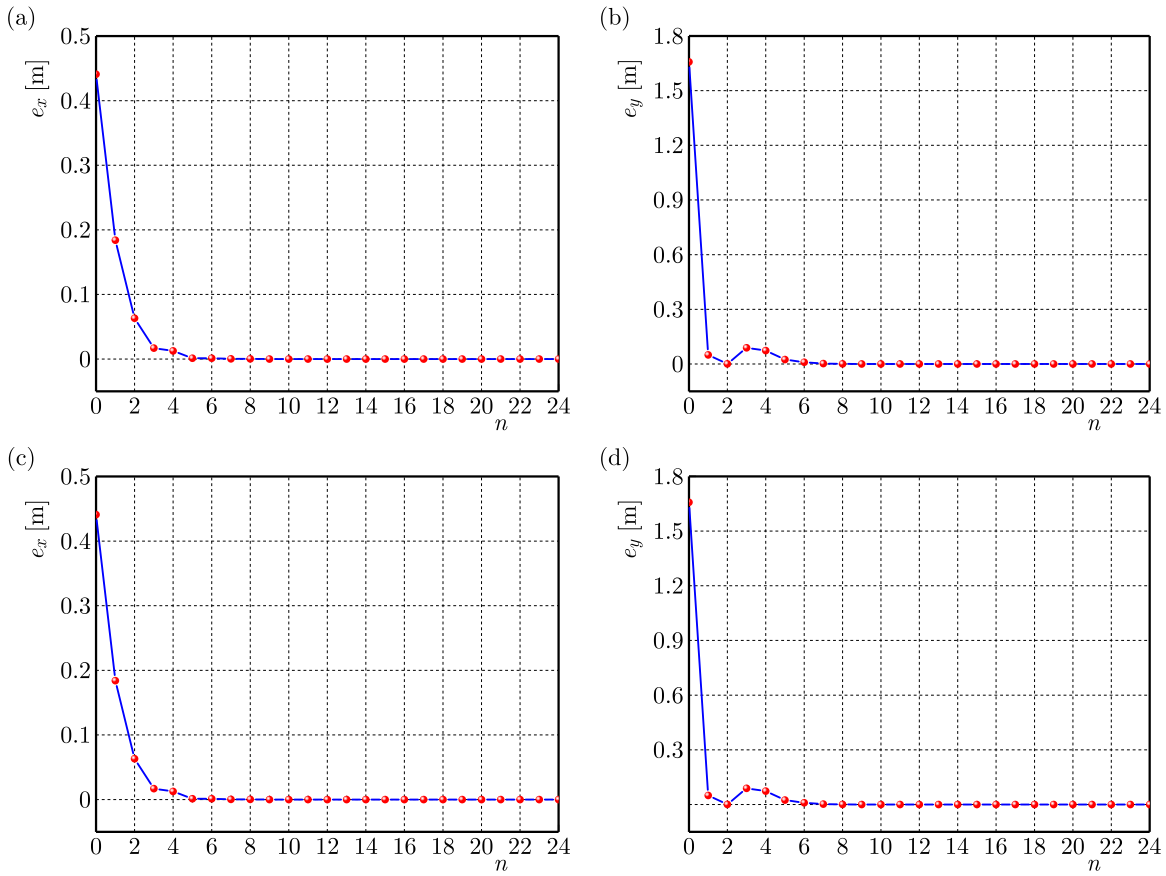

Fig. 2. Curve of error: (a) e_x ($x = 0$, $y = d$); (b) e_y ($x = 0$, $y = d$); (c) e_x ($x = \pm a$, $y = 0$); (d) e_x ($x = \pm a$, $y = 0$).

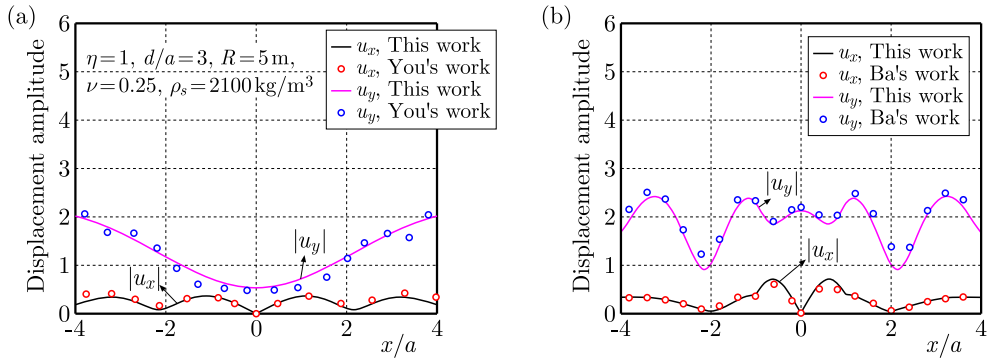

Fig. 3. Curve of comparative verification.

4. Analysis

The parameters (Zhang *et al.*, 2024) chosen in this research are exhibited in Table 1, the tunnel radius $a = 5$ m.

4.1. Impact of incident frequency on the diffraction of wave

Figure 4 shows the variety curves of the displacement amplitude at the water-soil interface and the DSCF of the tunnel surface when the incident angle $\theta_{ip1} = 30°$ and the incident wave frequencies are $\eta = 0.5$, 1, 2, respectively. It can be found out from the figure that the complex degree of the spatial pattern for the displacement increases along the frequency. The reason is

Table 1. Physical parameters.

Material parameters	Magnitude
Porosity n	0.3
Soil particle density ρ^S [kg/m^3]	2650
Liquid density ρ^L [kg/m^3]	1000
Bulk modulus of soil particles K_s [GPa]	36
Bulk modulus of liquid K_f [GPa]	2
Solid skeleton bulk modulus K [MPa]	43.6
Intrinsic permeability of the soil k [m^2]	3×10^{-13}
Viscosity coefficient of solid η^b [Pa · s]	1×10^{-3}
Permeability coefficient k^b [Pa · s]	1×10^{-10}
Lamé constant λ_S [MPa]	26.2
Lamé constant μ_S [MPa]	26.1

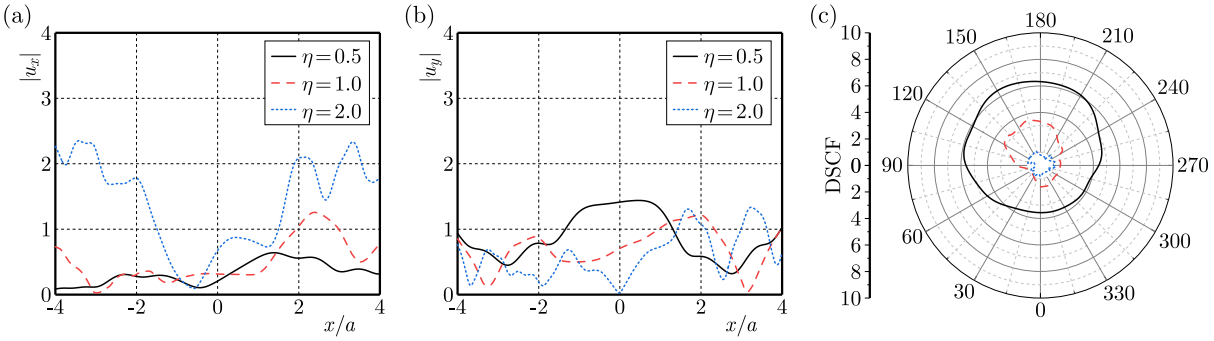

Fig. 4. Curves of displacement amplitude and DSCF at water-soil interface changing with frequency: (a) $|u_x|$; (b) $|u_y|$; (c) DSCF.

that when η is low, the incident wavelength is far above the tunnel radius, and it is insensitive to small terrain changes. Furthermore, the displacement on the left side changes more complexly than it does on the right side. The reason for this is the tunnel leading to the production of scattered waves. The left side of the tunnel reflects the wave. Scattering waves interfere with each other, causing energy convergence, so that the displacement curve at the water-soil interface appears as crests and valleys, exhibiting the characteristics of stationary waves (Cao & Lee, 1990; Lee & Cao, 1989; Lee & Karl, 2014). As the frequency increases, the number of crests and valleys in the figures increases, and the displacement alters more sharply, which shows that the interference effect of the wave is enhanced. As the frequency increases, the DSCF on the tunnel surface gradually decreases, and its distribution becomes more complex.

4.2. Impact of incident angle on the diffraction of wave

Figure 5 gives the displacement amplitude at the water-soil interface and the DSCF curve of the tunnel surface when the incident angle $\theta_{ip1} = 0°$, 30°, 60°, and incident frequency $\eta = 1$. It can be seen from the figures that when $\theta_{ip1} = 0°$, the displacement is symmetrical about $x = 0$. As the θ_{ip1} increases, the displacement on the left side changes more complexly than on the right one. Moreover, as the incident angle increases, both horizontal and vertical displacements as well as the peak value of DSCF decrease.

4.3. Impact of porosity on the diffraction of wave

Figure 6 illustrates the displacement and DSCF curves as the incident wave frequency is $\eta = 1$ and the porosity $n = 0.1$, 0.2, 0.3 gradually increases.

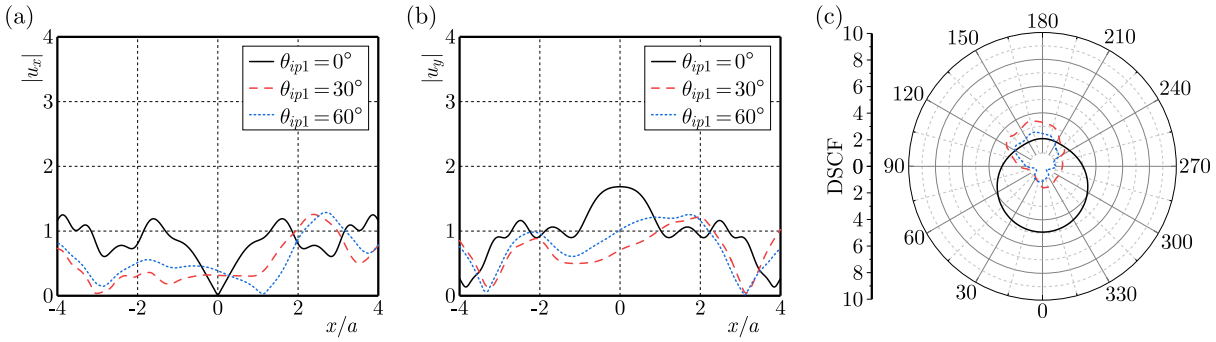

Fig. 5. Curves of displacement amplitude and DSCF at water-soil interface changing with angle: (a) $|u_x|$; (b) $|u_y|$; (c) DSCF.

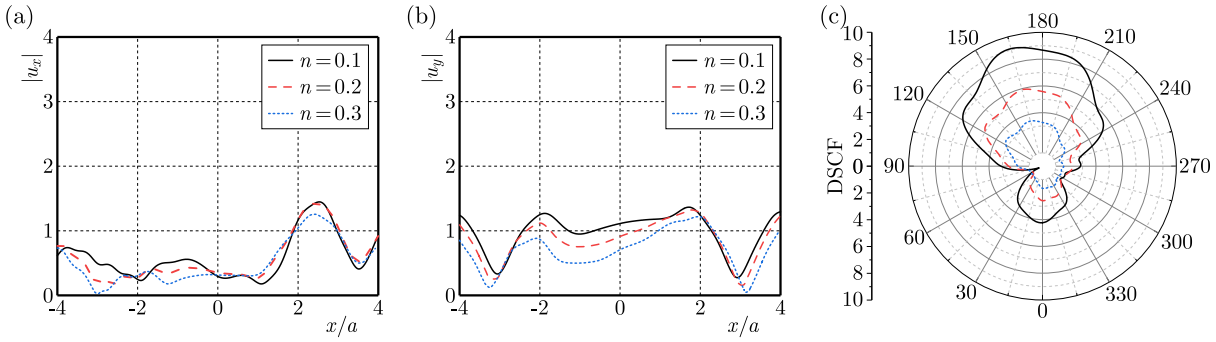

Fig. 6. Curves of displacement amplitude and DSCF at water-soil interface changing with porosity: (a) $|u_x|$; (b) $|u_y|$; (c) DSCF.

It can be found from the figures that as the porosity increases, the displacement at the water-soil interface, as well as the DSCF of the tunnel surface decreases.

4.4. Impact of incident frequency on the diffraction of wave

Figure 7 shows the displacement and DSCF curves when the buried depth is $d/a = 2$, 5, 10 in the case of $\theta_{ip1} = 30°$ and $\eta = 1$.

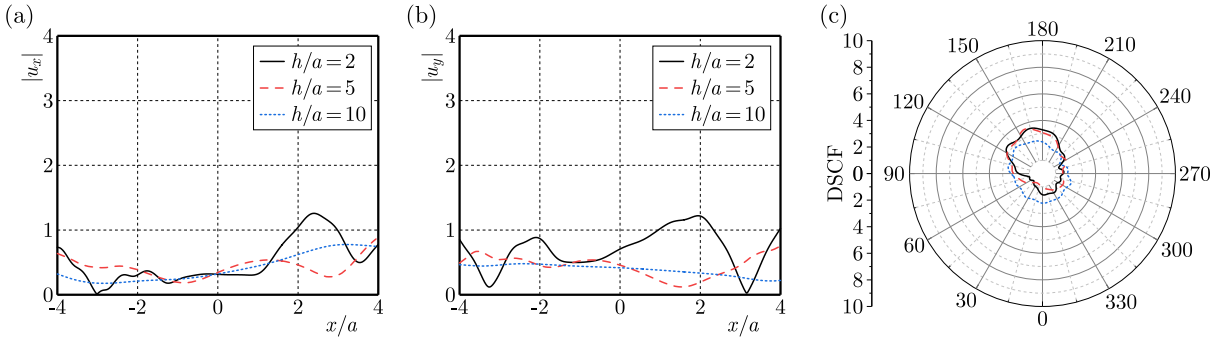

Fig. 7. Curves of displacement amplitude and DSCF at water-soil interface changing with burial depth: (a) $|u_x|$; (b) $|u_y|$; (c) DSCF.

With the increase of buried depth, the displacement at the water-soil interface decreases. However, the impact of the buried depth on the peak value of DSCF on the tunnel surface is not significant, and the DSCF at the top of the tunnel decreases as the buried depth increases. The DSCF at the bottom of the tunnel increases along with the buried depth.

5. Conclusion

Based on the Biot theory, the solution for P-wave scattering by underwater tunnel is given using the Fourier–Bessel series expansion. By numerical examples, the effect of incident angle, frequency, porosity and buried depth on displacement amplitude and dynamic stress concentration factor at the water-soil interface in the underwater tunnel is examined. The research indicates that:

1) The frequency has a considerable influence on the displacement at the water-soil interface and DSCF of the tunnel surface. The complex degree of the spatial pattern for the displacement increases along the incident frequency. The displacement amplitude inside the tunnel and at the water-soil interface on the left side changes greatly. It is extremely necessary to consider the impact of the incident wave frequency on the diffraction of the elastic wave in the underwater tunnel.
2) As the incident angle amplifies, the displacement on the left side changes more complexly compared to the right side, and the displacement amplitude and the peak value for DSCF decrease.
3) As the porosity amplifies, the displacement amplitude at the water-soil interface and the DSCF of the tunnel surface decrease.
4) The displacement amplitude at the water-soil interface decreases with the buried depth increase. The DSCF at the top of the tunnel decreases as the buried depth increases, and the DSCF at the bottom side increases with the increase of buried depth.

References

1. Achenbach, J.D. (1973). [Review of the book *Diffraction of Elastic Waves and Dynamic Stress Concentrations*, by Y.H. Pao & C.C. Mow]. *Journal of Applied Mechanics*, *40*, 872. https://doi.org/10.1115/1.3423178
2. Ba, Z. (2006). *Scattering of P and SV waves by canyons and tunnels in saturated half-space*. Tianjin University.
3. Ba, Z., Sang, Q., & Liang, J. (2022). Seismic analysis of a lined tunnel in a multi-layered TI saturated half-space due to qP1- and qSV-waves. *Tunnelling and Underground Space Technology*, 119, Article 104248. https://doi.org/10.1016/j.tust.2021.104248
4. Biot M.A. (1956a). Theory of propagation of elastic waves in a fluid-saturated porous solid. I. Low-frequency range. *The Journal of the Acoustical Society of America*, *28*(2), 168–178. https://doi.org/10.1121/1.1908239
5. Biot M.A. (1956b). Theory of propagation of elastic waves in a fluid-saturated porous solid: II. Higher frequency range. *The Journal of the Acoustical Society of America*, *28*(2), 179–191. https://doi.org/10.1121/1.1908241
6. Cao, H. & Lee, V.W. (1990). Scattering and diffraction of plane P waves by circular cylindrical canyons with variable depth-to-width ratio. *Soil Dynamics and Earthquake Engineering*, *9*(3), 141–150. https://doi.org/10.1016/S0267-7261(09)90013-6
7. Ding, H., Tong, L.H., Xu, C., & Hu, W. (2020). Aseismic performance analysis of composite lining embedded in saturated poroelastic half space. *International Journal of Geomechanics*, *20*(9), Article 04020156. https://doi.org/10.1061/(ASCE)GM.1943-5622.0001787
8. Gomes, R.C., Gouveia, F., Torcato, D., & Santos, J. (2015). Seismic response of shallow circular tunnels in two-layered ground. *Soil Dynamics and Earthquake Engineering*, *75*, 37–43. https://doi.org/10.1016/j.soildyn.2015.03.012
9. Kattis, S.E., Beskos, D.E., & Cheng, A.H.D. (2003). 2D dynamic response of unlined and lined tunnels in poroelastic soil to harmonic body waves. *Earthquake Engineering and Structural Dynamics*, *32*(1), 97–110. https://doi.org/10.1002/eqe.216

10. Lee, V.W. & Cao, H. (1989). Diffraction of SV waves by circular canyons of various depths. *Journal of Engineering Mechanics*, *115*(9), 2035–2056. http://dx.doi.org/10.1061/(ASCE)0733-9399(1989)115:9(2035)

11. Lee, V.W. & Karl, J. (1992). Diffraction of *SV* waves by underground, circular, cylindrical cavities. *Soil Dynamics & Earthquake Engineering*, *11*(8), 445–456. https://doi.org/10.1016/0267-7261(92)90008-2

12. Lee, V.W. & Liu, W.Y. (2014). Two-dimensional scattering and diffraction of P- and SV-waves around a semi-circular canyon in an elastic half-space: An analytic solution via a stress-free wave function. *Soil Dynamics and Earthquake Engineering*, *63*, 110–119. https://doi.org/10.1016/j.soildyn.2014.02.005

13. Liang, Y., Zhou, F., Cao, X., Wang, L., Liu, H., & Zhu, S. (2023). Scattering of plane SH waves by a circular tunnel in nonlocal fractional-order viscoelastic half-space. *Soil Dynamics and Earthquake Engineering*, *170*, Article 107934. https://doi.org/10.1016/j.soildyn.2023.107934

14. Liu, Z., Ju, X., Wu, C., & Liang, J. (2017). Scattering of plane P_1 waves and dynamic stress concentration by a lined tunnel in a fluid-saturated poroelastic half-space. *Tunnelling and Underground Space Technology*, *67*, 71–84. https://doi.org/10.1016/j.tust.2017.04.017

15. Luco, J.E. & de Barros, F.C.P. (1994). Dynamic displacements and stresses in the vicinity of a cylindrical cavity embedded in a half-space. *Earthquake Engineering and Structural Dynamics*, *23*(3), 321–340. https://doi.org/10.1002/eqe.4290230307

16. Ma, Q., Zhou, F.X., Shao, S.J., Shao, S., & Zhang, M. (2023). Diffraction of plane P waves by a circular-arc canyon in an unsaturated poroelastic half-space. *Soil Dynamics and Earthquake Engineering*, 174, Article 108163. https://doi.org/10.1016/j.soildyn.2023.108163

17. Tan, Y., Yang, M., & Li, X. (2020). Dynamic response of a circular lined tunnel with an imperfect interface embedded in the unsaturated poroelastic medium under P wave. *Computers and Geotechnics*, *122*, Article 103514. https://doi.org/10.1016/j.compgeo.2020.103514

18. Xiang, G.L., Tao, M., Zhao, R., Zhao, H., Memon, M.B., & Wu, C. (2024). Dynamic response of water-rich tunnel subjected to plane P wave considering excavation induced damage zone. *Underground Space*, *15*, 113–130. https://doi.org/10.1016/j.undsp.2023.08.010

19. Xu, C.J., Ding, H.B., Tong, L.H., Luo, W.J., & Wang, N. (2019). Scattering of a plane wave by shallow buried cylindrical lining in a poroelastic half-space. *Applied Mathematical Modelling*, *70*, 171–189. https://doi.org/10.1016/j.apm.2019.01.029

20. You, H.B. (2005). *Elastic wave scattering by a canyon or tunnel in layered saturated half space* (in Chinese). Tianjin University.

21. Yue, C. & Liu, Q. (2023). Dynamic response of a shallow lined circular tunnel by incident P1 and SV waves in an unsaturated half-plane. *Tunnelling and Underground Space Technology*, *141*, Article 105364. https://doi.org/10.1016/j.tust.2023.105364

22. Zhang, J.L., Ma, Q., & Jiang, H.P. (2024). Study on the transmission and reflection of P1 wave at the interface between saturated soil and saturated frozen soil medium (in Chinese). *Rock and Soil Mechanics*, *45*(10), 1–14.

23. Zhao, S. & Ma, Q. (2024). Diffraction of plane P waves by a circular unlined tunnel in an unsaturated poroelastic half-space. *Journal of Vibration Engineering & Technologies*, *12*(Suppl. 2), 1501–1519. https://doi.org/10.1007/s42417-024-01487-w

24. Zhao, S., Ma, Q., & Zhang, W.Y. (2024). Diffraction of plane P-waves by a single-layer lined tunnel in an unsaturated poroelastic half-space. *Mechanics of Solids*, *59*(1), 496–520. https://doi.org/10.1134/S0025654424600041

25. Zhou, F.X., Lai, Y.M., & Song, R.X. (2013). Propagation characteristics of plane wave in non-homogeneously saturated soils (in Chinese). *Science China Press*, *43*(2), 131–140.

Manuscript received September 27, 2024; accepted for publication January 29, 2025; published online March 24, 2025.